Theoretical and Applied Fracture Mechanics 121 (2022) 103438

Contents lists available at ScienceDirect

Theoretical and Applied Fracture Mechanics

journal homepage: www.elsevier.com/locate/tafmec

Closed-form equations for the calculation of stress intensity factors for embedded cracks in round bars subjected to tensile load

J.M. Alegre *, I.I. Cuesta, A. Díaz

University of Burgos, Escuela Politécnica Superior, Av de Cantabria s/n, Burgos 09006, Spain

ARTICLE INFO

Keywords:
Stress intensity factor
Embedded elliptical cracks
Fatigue

ABSTRACT

Fatigue crack propagation initiated from internal defects is a typical mechanism observed in high cycle fatigue (HCF) and very high cycle fatigue (VHCF) of cylindrical tensile specimens subjected to uniaxial cyclic loads. To study the fatigue crack propagation of these embedded cracks by means of a fracture mechanics approach, solutions for the Stress Intensity Factor (SIF) for different crack configurations are needed. In this paper, a set of closed-form equations for the calculation of the SIF of embedded cracks in round bars subjected to tensile load is presented. Two sets of solutions are provided, which allow for different levels of approach to be considered. The first solution provides the SIF for the vertex points of an internal elliptical crack as a function of three dimensionless parameters related to crack size, crack position and crack aspect ratio. The second solution is a simplification for eccentric circular cracks located at any position of the cross section. The methodology necessary for the application to the study of fatigue crack propagation is also presented, and a comparison with those obtained from experimental tests is included, which exhibits a very good capacity for prediction.

1. Introduction

Fatigue crack initiation in high cycle fatigue (HCF) and very high cycle fatigue (VHCF) regimes of round bars subjected to tensile loads are often linked to the presence of internal defects or microstructural features (Fig. 1). The fatigue crack propagation of these internal defects in round bars tends towards a circular shape, regardless of the irregular shape of the initiating defect, forming a characteristic circular crack pattern on the fracture surface known as a *fish-eye* [1–3]. To study the fatigue crack propagation of these embedded cracks by means of a fracture mechanics approach, the Stress Intensity Factor (SIF) for embedded elliptical cracks in round bars is needed.

From the pioneer studies of Green [4] and Irwin [5,6] for an embedded elliptical crack in an infinite solid subjected to uniform uniaxial stress, a great number of papers can be found in the literature dedicated to embedded elliptical cracks in different geometries. For the case of embedded elliptical cracks in plates, some papers have been included as a reference for most design codes, such as the solution of Varfolomeev and Vainshtok [7], Newman and Raju [8] or Isida and Noguchi [9], among others.

For the case of internal flaws in round bars, only a few solutions for the SIF can be found in the literature [10–14], and most of them focused on centered, penny-shaped cracks. Nishioka and Atluri [13] evaluate a round bar with an embedded circular crack located at the center of the bar and subjected to pure tension or pure bending at the ends of the bar. Benthem *et al* [14] also provide the stress-intensity factor solution for a circular embedded crack (centered) in a round bar and subjected to tensile, bending and torsion loads. This last solution is given in the FITNET code of practice [15] and in the FKM guideline [16].

In a previous paper by the authors [17], a tabulated solution for the SIF of embedded elliptical cracks in round bars subjected to tensile load was presented. The solutions were obtained from a 3D finite element analysis and enable the ability to obtain the SIF as a function of three dimensionless parameters (crack size, crack aspect ratio and crack position in the cross section), covering ranges for most internal crack shapes in practice to be analyzed. However, these tabulated solutions are quite laborious to use for evaluation purposes due to the necessity to carry out complex interpolations that require the development of programming tools.

In this way, the novelty of this paper lies in the development of a set of closed-form solutions for the calculation of the SIF of embedded cracks in round bars subjected to uniaxial tensile load, which allow researchers and designers to be able to use these SIF solutions without the necessity to carry out laborious and complex interpolations of the

* Corresponding author.
E-mail address: jalegre@ubu.es (J.M. Alegre).

https://doi.org/10.1016/j.tafmec.2022.103438
Received 3 February 2022; Received in revised form 6 June 2022; Accepted 6 June 2022
Available online 9 June 2022

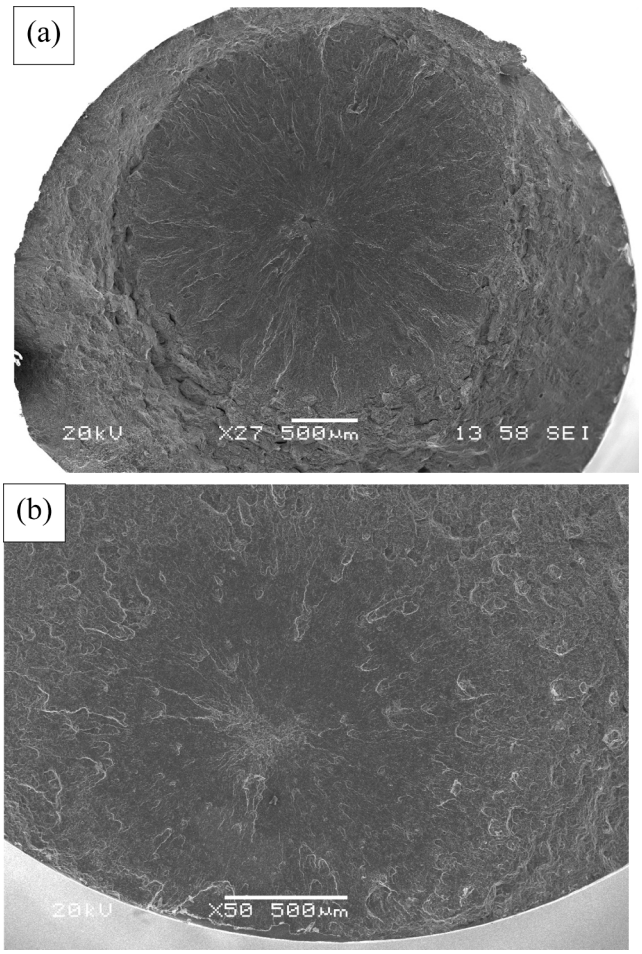

Fig. 1. Fish-eye examples initiated by fatigue in a round bar: (a) from an internal defect, lack-of-fusion type, on a Ti-6Al4V alloy fabricated by selective laser melting, and (b) from microstructural facets formed in a wrought processed Ti-6Al-4V.

tabulated solutions. This is a highly desirable practice for SIF solutions. The proposed solution is based on a combination of a nonlinear three-parameter equation and polynomial equations, that allows to adequately fit the evolution of the geometry correction factors over the whole range of application. The accuracy obtained is very good compared to the previous tabulated solutions.

Two different types of solutions are provided, which are useful for different levels of analysis. The first solution provides the SIF for the vertex points of an internal elliptical crack as a function of three dimensionless parameters related to the crack size, crack position, and crack aspect ratio. The second solution is a simplification for eccentric circular cracks located at any position of the cross section.

Moreover, a typical sequential methodology for fatigue crack growth simulation is presented, one that considers an elliptical crack shape evolution during fatigue process using the SIF values at the vertices of the elliptical crack. Some examples of its use for the simulation of fatigue crack propagation are also included in the last section of this paper.

2. Geometry definition and sif tabulated solutions

The geometry and main dimensions of the embedded elliptical crack in a round bar considered in this study are presented in Fig. 2, where R is the radius of the bar and σ_0 the tensile applied stress. The elliptical crack size and crack position are defined by the semi-axis of the ellipse (a and c) and the position of the center of the crack ($a + h$). Three dimensionless parameters are defined that consider the relative position of the

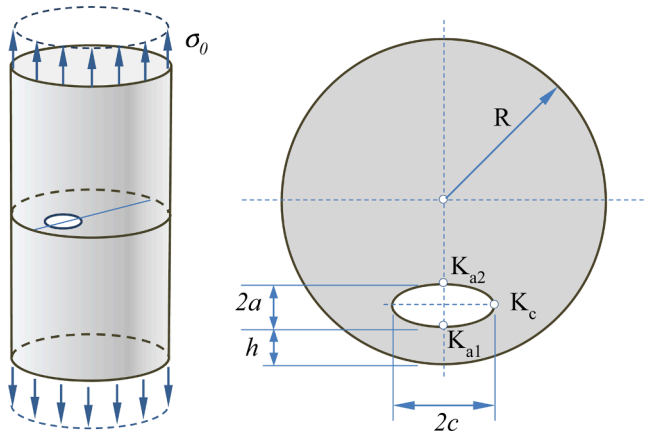

Fig. 2. Geometry definition of the embedded elliptical crack in a round bar for a general case.

crack $(a + h)/R$, the ratio of crack size versus the distance from the center of the ellipse to the surface $a/(a+h)$ and the crack aspect ratio of the elliptical crack a/c.

The stress-intensity factors for this geometry were obtained from a 3D finite element model using Abaqus software. Due to the symmetry of the problem, only one-fourth of the round bar was modelled by employing 20-node quadratic elements with reduced integration (C3D20R). Quarter-point wedge finite elements were used around the crack front to model the stress field singularity. A mesh density of 8 elements for the semi-rosette of the crack tip was chosen, and the crack front was constructed with 100 elements. Specific details and a validation of this model can be found in a previous paper by the authors [17].

The SIF at the vertices of the elliptical crack (Fig. 2) can be calculated as:

$$\begin{aligned} K_{a1} &= F_{a1}\cdot\sigma_0\cdot\sqrt{\pi a} \\ K_{a2} &= F_{a2}\cdot\sigma_0\cdot\sqrt{\pi a} \\ K_c &= F_c\cdot\sigma_0\cdot\sqrt{\pi a} \end{aligned} \tag{1}$$

where F_{a1}, F_{a2} and F_c are the geometry correction factors.

In order to cover most situations in practice, these geometry correction factors were calculated as a function of three dimensionless parameters: $a/(a+h)$ ranging from 0.05 to 0.95, $(a+h)/R$ ranging from 1 to 0.05 and a/c ranging from 0.2 to 1.0. The calculated values are collected on Tables 1–3 respectively. Non tabulated values correspond to situations that are not geometrically possible for the crack geometry within the section.

3. Closed-form equations for embedded elliptical cracks

In this section, the closed-form equations are presented for the most general case, i.e. an elliptical crack located at any position of the circular cross section. The closed-form equations provide the geometry correction factors with which the SIF can be obtained by applying the previous equation (1). A non-linear growth curve with 3 parameters (B_i,C_i,m_i) has been chosen to reproduce the observed trend of the geometry correction factors for each set of values as a function of $a/(a + h)$. This sort of equation shows the general form presented in equation (2) and makes it possible to appropriately reproduce the initial horizontal asymptote for values of $a/(a+h)\to 0$ controlled by B_1, the growth shape controlled by the exponent m_1 and the upper value for $a/(a+h)\to 1$ controlled by $B_1/(1 - C_1)$. An example of the effect of each of the three parameters on the curve shape is shown in Fig. 3.

The geometry correction factor F_{a1} can be then obtained as:

$$F_{a1} = \frac{B_1}{1 - C_1\cdot\left(\frac{a}{a+h}\right)^{m_1}} \tag{2}$$

Table 1
Geometry correction factor, F_{a1}.

a/c	$\frac{a}{(a+h)}$	0.05	0.2	$(a+h)/R$ 0.4	0.6	0.8	1.0
0.2	**0.05**	0.9481	0.9481	0.9481	0.9481	0.9481	0.9481
	0.2	0.9531	0.9543	0.9582	0.9636	0.9695	–
	0.4	0.9834	0.9967	–	–	–	–
	0.6	1.0649	–	–	–	–	–
	0.8	1.2756	–	–	–	–	–
	0.95	1.9484	–	–	–	–	–
0.4	**0.05**	0.8665	0.8665	0.8665	0.8665	0.8665	0.8665
	0.2	0.8689	0.8694	0.8704	0.8722	0.8744	0.8784
	0.4	0.8871	0.8918	0.9068	0.9285	0.9521	–
	0.6	0.9422	0.9635	1.0347	–	–	–
	0.8	1.0790	1.1586	–	–	–	–
	0.95	1.5754	–	–	–	–	–
0.6	**0.05**	0.7812	0.7812	0.7812	0.7812	0.7812	0.7812
	0.2	0.7823	0.7825	0.7828	0.7835	0.7844	0.7862
	0.4	0.7942	0.7966	0.8029	0.8136	0.8250	0.841
	0.6	0.8317	0.8421	0.8753	0.9262	0.9822	–
	0.8	0.9405	0.9765	1.1007	1.3091	–	–
	0.95	1.2667	1.3855	1.8561	–	–	–
0.8	**0.05**	0.7058	0.7058	0.7058	0.7058	0.7058	0.7058
	0.2	0.7067	0.7068	0.7069	0.7072	0.7076	0.7082
	0.4	0.7146	0.7159	0.7191	0.7246	0.731	0.7396
	0.6	0.7413	0.7474	0.7645	0.7927	0.8216	0.8532
	0.8	0.8216	0.8419	0.9063	1.0135	1.1406	–
	0.95	1.0669	1.1293	1.3360	1.7603	–	–
1	**0.05**	0.6386	0.6386	0.6386	0.6386	0.6386	0.6386
	0.2	0.6388	0.6388	0.6389	0.6391	0.6394	0.6398
	0.4	0.6437	0.6446	0.6463	0.6492	0.6529	0.6582
	0.6	0.6631	0.6671	0.6769	0.6936	0.7108	0.7274
	0.8	0.7239	0.7368	0.7731	0.8347	0.8998	0.9525
	0.95	0.9143	0.9520	1.0637	1.2671	1.5391	1.8441

$$m_1 = 1.74\left(\frac{a}{c}\right) + (2.0979\cdot\lambda^3 - 2.4414\cdot\lambda^2 - 1.1883\cdot\lambda + 3.7175)$$

$$B_1 = 0.0691\cdot\left(\frac{a}{c}\right)^2 - 0.4728\cdot\left(\frac{a}{c}\right) + 1.0416$$

$$C_1 = M_2\cdot\left(\frac{a}{c}\right)^2 + M_1\cdot\left(\frac{a}{c}\right) + M_0$$

$$M_2 = -1.6458\cdot\lambda^4 + 4.7320\cdot\lambda^3 - 4.9173\cdot\lambda^2 + 3.1147\cdot\lambda - 0.03859$$

$$M_1 = -1.6880\cdot\lambda^4 + 1.2160\cdot ON$$

$$\lambda^3 + 1.7455\cdot\lambda^2 - 4.3137\cdot\lambda - 0.2057$$

$$M_0 = 3.1480\cdot\lambda^4 - 6.1104\cdot\lambda^3 + 3.8745\cdot\lambda^2 + 1.2555\cdot\lambda + 0.6319$$

$$\lambda = \frac{a+h}{R}$$

The geometry correction factor F_{a2} can be obtained as:

$$F_{a2} = \frac{B_2}{1 - C_2\cdot\left(\frac{a}{a+h}\right)^{m_2}} \tag{3}$$

$$m_2 = 1.8919\cdot\lambda + 2.0296$$

$$B_2 = 0.0707\cdot\left(\frac{a}{c}\right)^2 - 0.4742\cdot\left(\frac{a}{c}\right) + 1.0414$$

$$C_2 = H_2\cdot\left(\frac{a}{c}\right)^2 + H_1\cdot\left(\frac{a}{c}\right) + H_0$$

$$H_2 = -38.5367\cdot\lambda^5 + 121.5224\cdot\lambda^4 - 104.8934\cdot\lambda^3 + 37.2244\cdot\lambda^2 - 4.2940\cdot\lambda + 0.2228$$

$$H_1 = 36.8200\cdot\lambda^5 - 158.9202\cdot\lambda^4 + 152.4389\cdot\lambda^3 - 59.5097\cdot\lambda^2 + 6.9928\cdot\lambda - 0.4675 H_0 = 12.0938\cdot\lambda^5 + 17.2795\cdot\lambda^4 - 33.8472\cdot\lambda^3 + 18.6236\cdot\lambda^2 - 2.2129\cdot\lambda + 0.2624$$

And finally, the geometry correction factor F_c can be obtained as:

$$F_c = \frac{B_3}{1 - C_3\cdot\left(\frac{a}{a+h}\right)^{m_3}} \tag{4}$$

$$m_3 = 1.6287\cdot\lambda^3 - 2.8580\cdot\lambda^2 + 2.7763\cdot\lambda + 2.3625$$

$$B_3 = 0.5135\cdot\left(\frac{a}{c}\right)^3 - 1.4051\cdot\left(\frac{a}{c}\right)^2 + 1.3199\cdot\left(\frac{a}{c}\right) + 0.2105$$

$$C_3 = G_2\cdot\left(\frac{a}{c}\right)^2 + G_1\cdot\left(\frac{a}{c}\right) + G_0$$

$$G_2 = 32.9938\cdot\lambda^4 - 43.1064\cdot\lambda^3 + 16.8509\cdot\lambda^2 + 1.3102\cdot\lambda - 0.0249$$

$$G_1 = -81.7186\cdot\lambda^4 + 118.4910\cdot\lambda^3 - 57.1224\cdot\lambda^2 + 2.9721\cdot\lambda - 0.1924$$

$$G_0 = 51.3498\cdot\lambda^4 - 79.5268\cdot\lambda^3 + 42.7400\cdot\lambda^2 - 4.5145\cdot\lambda + 0.2993$$

The accuracy of the fit comparing the tabulated solutions obtained from 3D finite element analysis to the closed-form equations is shown in Fig. 4. In general, a very good agreement is obtained, with a difference less than 1%, except for some particular values corresponding to extreme situations (such as cracks very close to the surface or with an

Table 2
Geometry correction factor, F_{a2}.

a/c	$\frac{a}{(a+h)}$	0.05	0.2	$(a+h)/R$ 0.4	0.6	0.8	1.0
0.2	**0.05**	0.9481	0.9481	0.9481	0.9481	0.9481	0.9481
	0.2	0.9521	0.9531	0.9564	0.9608	0.9663	–
	0.4	0.9692	0.9796	–	–	–	–
	0.6	1.0025	–	–	–	–	–
	0.8	1.0436	–	–	–	–	–
	0.95	1.0870	–	–	–	–	–
0.4	**0.05**	0.8663	0.8663	0.8663	0.8663	0.8663	0.8664
	0.2	0.8679	0.8683	0.8692	0.8705	0.8726	0.8781
	0.4	0.8775	0.8808	0.8917	0.9058	0.9256	–
	0.6	0.8951	0.9101	0.9539	–	–	–
	0.8	0.9214	0.9615	–	–	–	–
	0.95	0.9662	–	–	–	–	–
0.6	**0.05**	0.7804	0.7804	0.7804	0.7804	0.7804	0.7804
	0.2	0.7815	0.7813	0.7816	0.7823	0.7839	0.7866
	0.4	0.7882	0.7897	0.7941	0.7995	0.8102	0.8414
	0.6	0.8001	0.8059	0.8241	0.8499	0.8890	–
	0.8	0.8191	0.8354	0.8915	0.9675	–	–
	0.95	0.8357	0.8698	1.0040	–	–	–
0.8	**0.05**	0.7067	0.7067	0.7067	0.7067	0.7067	0.7067
	0.2	0.7071	0.7071	0.7072	0.7074	0.7078	0.7087
	0.4	0.7104	0.7112	0.7131	0.7163	0.7217	0.7402
	0.6	0.7182	0.7213	0.7306	0.7421	0.7637	0.8538
	0.8	0.7304	0.7385	0.7657	0.8001	0.8611	–
	0.95	0.7409	0.7568	0.8129	0.8929	–	–
1	**0.05**	0.6387	0.6386	0.6386	0.6386	0.6386	0.6386
	0.2	0.6392	0.6392	0.6393	0.6395	0.6398	0.6398
	0.4	0.6409	0.6413	0.6422	0.6439	0.6467	0.6582
	0.6	0.6462	0.6479	0.6527	0.6598	0.6719	0.7274
	0.8	0.6543	0.6589	0.6732	0.6913	0.7237	0.9525
	0.95	0.6584	0.6669	0.6959	0.7296	0.7912	1.8441

elongated geometry) where the difference is still always less than 3%.

4. Closed-form equations for eccentric circular cracks

The particular case of an embedded circular crack located at any position of the cross section is of great interest due to its simplicity and applicability. A scheme of the crack geometry for this particular case is shown in Fig. 5. It has been experimentally observed that, for this geometry, an initial internal flaw tends towards a circular shape during its growth forming a characteristic pattern known as a fish-eye (Fig. 1). Furthermore, the irregular shape of the initiating defect can be converted into an equivalent circular one, using the $\sqrt{area}$ parameter model of Murakami [18], which produces the same fatigue life [19]. Consequently, an analysis of fatigue crack propagation in this geometry can be performed with a very good approximation, assuming a circular initial crack and a circular fatigue crack growth. In this case, only the SIF for the two opposite endpoints of the crack in the radial direction are needed (i.e. K_{a1} and K_{a2}).

The closed-form equations for this case can be derived using the general closed-form equations for F_{a1} and F_{a2}, presented in Eqs. (2) and (3) respectively, particularized for $a/c = 1$. In this way, the next set of closed-form equations can be derived:

$$\begin{aligned} F_{a1} &= \frac{B_1}{1 - C_1 \cdot \left(\frac{a}{a+h}\right)^{m_1}} \\ B_1 &= 0.6379 \\ m_1 &= 2.0979 \cdot \lambda^3 - 2.4414 \cdot \lambda^2 - 1.1883 \cdot \lambda + 5.4575 \\ C_1 &= -0.1859 \cdot \lambda^4 - 0.1624 \cdot \lambda^3 + 0.7027 \cdot \lambda^2 + 0.0566 \cdot \lambda + 0.3876 \end{aligned} \tag{5}$$

$$\begin{aligned} F_{a2} &= \frac{B_2}{1 - C_2 \cdot \left(\frac{a}{a+h}\right)^{m_2}} \\ B_2 &= 0.6379 \\ m_2 &= 1.8919 \cdot \lambda + 2.0296 \\ C_2 &= \begin{array}{c} 10.3772 \cdot \lambda^5 - 20.1183 \cdot \lambda^4 + 13.6983 \cdot \lambda^3 \\ -3.6619 \cdot \lambda^2 + 0.4858 \cdot \lambda + 0.0178 \end{array} \end{aligned} \tag{6}$$

5. Fatigue crack growth methodology

The simulation of the fatigue crack growth can be carried out using the previous closed-form equations and a sequential methodology. For a general case, the crack is continuously updated during fatigue, assuming an elliptical growth and, consequently, calculating the SIFs at the vertices of the semi-axis of the elliptical crack.

The first step is to define the initial crack size (a and c) and its position in the cross section ($a + h$). The three dimensionless parameters ($a/(a + h)$, $(a+h)/R$ and a/c) can be obtained and then the three geometry correction factors (F_{a1}, F_{a2}, F_c) can be calculated using the closed-form equations. Next, for a defined stress range $\Delta\sigma$ the stress-intensity factor ranges at the vertices of the elliptical crack are obtained as:

$$\begin{aligned} \Delta K_{a1} &= F_{a1} \cdot \Delta\sigma \cdot \sqrt{\pi a} \\ \Delta K_{a2} &= F_{a2} \cdot \Delta\sigma \cdot \sqrt{\pi a} \\ \Delta K_c &= F_c \cdot \Delta\sigma \cdot \sqrt{\pi a} \end{aligned} \tag{7}$$

Assuming a fatigue crack growth law (e.g. Paris law, $da/dN = C \cdot \Delta K^m$), the crack advance of the vertices of the ellipse is predicted after a user-defined block of cycles as:

Table 3
Geometry correction factor, F_c.

a/c	$\frac{a}{(a+h)}$	0.05	0.2	$(a+h)/R$ 0.4	0.6	0.8	1.0
0.2	**0.05**	0.4221	0.4221	0.4221	0.4221	0.4221	0.4221
	0.2	0.4236	0.4242	0.4260	0.4291	0.4353	–
	0.4	0.4284	0.4363	–	–	–	–
	0.6	0.4377	–	–	–	–	–
	0.8	0.4545	–	–	–	–	–
	0.95	0.4720	–	–	–	–	–
0.4	**0.05**	0.5477	0.5476	0.5478	0.5478	0.5478	0.5479
	0.2	0.5489	0.5492	0.5499	0.5510	0.5525	0.5559
	0.4	0.5550	0.5578	0.5669	0.5816	0.6100	–
	0.6	0.5666	0.5789	0.6281	–	–	–
	0.8	0.5833	0.6221	–	–	–	–
	0.95	0.6009	–	–	–	–	–
0.6	**0.05**	0.6057	0.6055	0.6057	0.6057	0.6058	0.6058
	0.2	0.6064	0.6065	0.6068	0.6072	0.6079	0.6098
	0.4	0.6120	0.6135	0.6179	0.6252	0.6349	0.6582
	0.6	0.6235	0.6299	0.6514	0.6870	0.7529	–
	0.8	0.6429	0.6624	0.7376	0.9221	–	–
	0.95	0.6567	0.7067	0.9238	–	–	–
0.8	**0.05**	0.6314	0.6314	0.6315	0.6315	0.6315	0.6315
	0.2	0.6318	0.6319	0.6320	0.6322	0.6325	0.6333
	0.4	0.6360	0.6370	0.6393	0.6434	0.6492	0.6623
	0.6	0.6464	0.6504	0.6623	0.6820	0.7090	0.7793
	0.8	0.6642	0.6756	0.7153	0.7835	0.9081	–
	0.95	0.6798	0.7099	0.8018	1.0052	–	–
1	**0.05**	0.6386	0.6386	0.6386	0.6386	0.6386	0.6386
	0.2	0.6389	0.6389	0.6390	0.6392	0.6395	0.6398
	0.4	0.6417	0.6423	0.6436	0.6459	0.6495	0.6582
	0.6	0.6504	0.6531	0.6602	0.6725	0.6889	0.7274
	0.8	0.6660	0.6736	0.6972	0.7367	0.7926	0.9525
	0.95	0.6861	0.6965	0.7487	0.8423	1.0031	1.8441

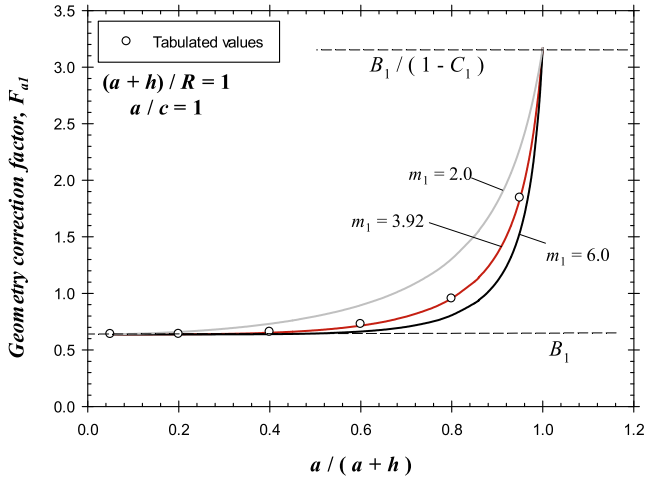

Fig. 3. Effect of the three parameters on the shape of the selected non-linear growth curve.

$$\begin{aligned}\Delta a_1 &= \Delta N \cdot C \cdot (\Delta K_{a1})^m \\ \Delta a_2 &= \Delta N \cdot C \cdot (\Delta K_{a2})^m \\ \Delta c &= \Delta N \cdot C \cdot (\Delta K_c)^m\end{aligned} \tag{8}$$

Where C and m are the Paris law coefficients and ΔN is the number of cycles per block chosen by the analysts. Accordingly, the selected value for ΔN makes it possible to control the number of calculated crack paths of the solution. Finally, the new crack size and crack position are updated by means of:

$$\begin{aligned}2a_{new} &= 2a + (\Delta a_1 + \Delta a_2) \\ 2c_{new} &= 2c + 2\Delta c \\ h_{new} &= h - \Delta a_1\end{aligned} \tag{9}$$

Using the calculated values from Eq. (9), a new crack front is constructed, which is assumed as a new elliptical shape of dimensions ($2a_{new}$ and $2c_{new}$) and the position of the center defined by ($h_{new} + a_{new}$).

As an alternative to the presented procedure, the crack advance at a certain point (e.g. Δa_1) can be used as the control parameter for crack propagation. In this way, the value of the number of cycles required for this advance (ΔN) is obtained from the first expression included in Eq. (8). Once this value of ΔN is obtained for this step, the advance of the rest of the points of interest of the crack front (Δa_2 and Δc) are calculated by means of the second and third expressions of Eq. (8) respectively.

The two approaches discussed above, based on Δa_1 or ΔN as control parameters, can be used to integrate the propagation law. There is no a predefined value that can be considered as a standard for selecting the interval size of Δa_1 or ΔN. A good practice is to perform a sensitivity analysis, setting an initial value (initial integration interval) and decreasing this value until no significant variation is observed between the solutions obtained.

Fig. 6 shows the propagation procedure explained before, where the new position of the elliptical crack vertices is obtained, allowing one to define a new elliptical crack front for the next analysis step. The whole procedure is repeated, updating the crack shape for each block of cycles (or crack point advance), until the failure condition is reached or the desired number of cycles is completed.

Assuming a circular crack shape during propagation a simplified analysis could be done. In this way, only the values of K_{a1} and K_{a2} are

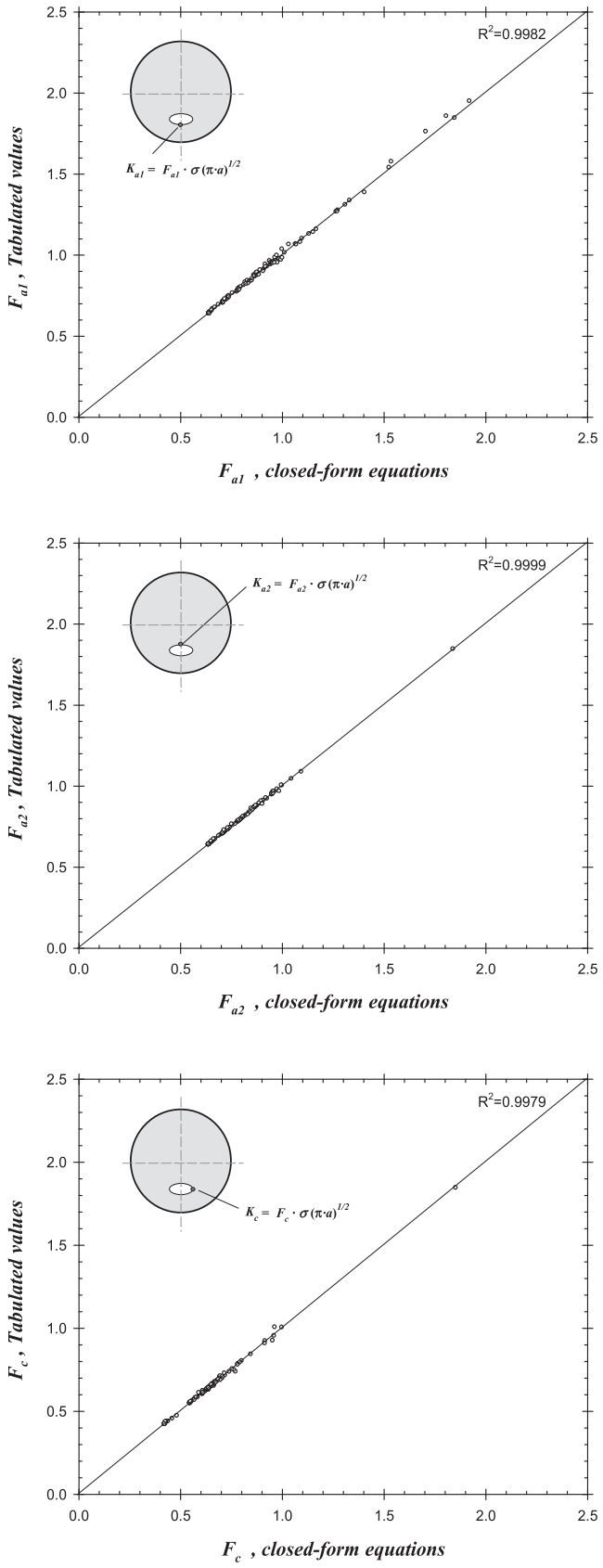

Fig. 4. Agreement between closed-form equations and tabulated values for the three geometry correction factors.

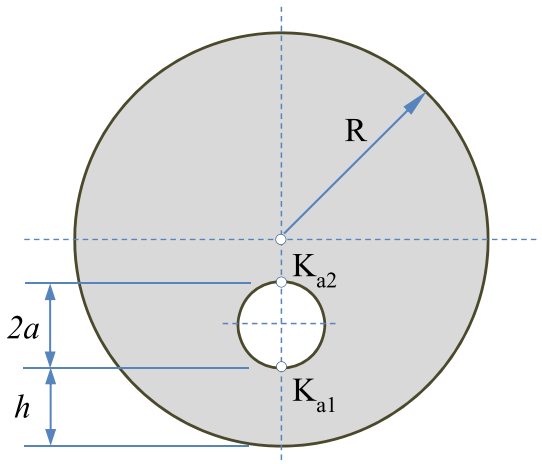

Fig. 5. Eccentric circular crack geometry.

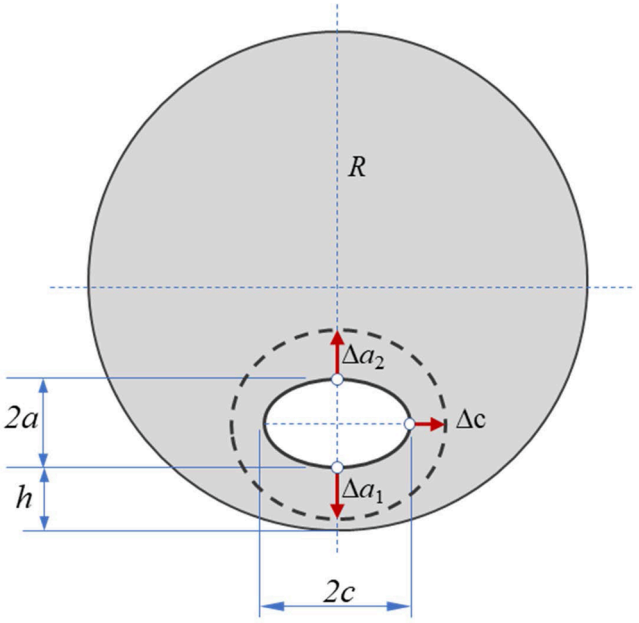

Fig. 6. Diagram of the procedure followed for the prediction of the new crack front.

calculated, using the geometry correction factors (F_{a1}, F_{a2}) from the simplified closed-form equations presented on (5) and (6). The values of Δa_1 and Δa_2 are calculated, and the new crack size and position is updated by $2a_{new}$ and h_{new}.

6. Application examples

This section contains some examples of application of the proposed closed-form equations for the prediction of fatigue propagation paths initiated from internal defects, with the objective to show its robustness for the fatigue crack growth prediction.

The first example is presented Fig. 7, which correspond to the same specimen shown in Fig. 1(a). The proposed closed-form equations for the SIF calculation, combined with the sequential methodology for fatigue crack growth presented in the earlier section, allows for a good prediction of the fatigue crack propagation during the fatigue process until the final crack shape is reached. The specimen displayed corresponds to a uniaxial fatigue test of a Ti-6Al-4V alloy fabricated by Selective Laser Melting (SLM). This Additive Manufacturing technique is generally

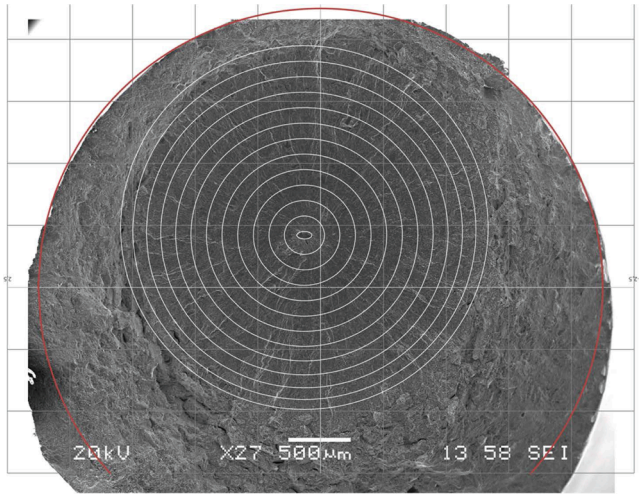

Fig. 7. Crack paths evolution, calculated from an internal initial defect (only a few paths are presented for clarity).

characterized by the presence of internal defects (lack-of-fusion) which are the origin of the fatigue crack propagation. The radius of the specimen was $R = 2.25$ mm, the uniaxial applied stress was $\Delta\sigma = 400\,MPa$ with a stress ratio of $\sigma_{min}/\sigma_{max} = 0$. The initial crack considered was defined by $a_0 = 0.03\,mm$ and $c_0 = 0.06$ mm, and its position in the circular cross section was defined by $h_0 = 1.75$ mm. The fatigue crack propagation law for this material was assumed to be a Paris type equation ($C = 3.5{\cdot}10^{-8}$ and $m = 2.1$, being ΔK in $MPa{\cdot}m^{1/2}$ and da/dN in $mm/cycle$) according to the experimental results obtained by de Jesus *et al* [20]. The control parameter for crack advance calculations was $\Delta a_1 = 0.005$ mm. Only a few paths are presented for clarity.

Fig. 8 shows a detail of the first steps of propagation from the initial irregularly shaped defect. For this case the radius of the specimen was also $R = 2.25$ mm, and the uniaxial applied stress was $\Delta\sigma = 400\,MPa$ with a stress ratio of $\sigma_{min}/\sigma_{max} = 0$. The initial crack size considered in this example was $a_0 = 0.03$ mm and $c_0 = 0.09$ mm. Its position in the circular cross section was defined by $h_0 = 1.32$ mm. One path is displayed for every ten calculated with $\Delta a_1 = 0.0025$ mm for clarity. The fatigue crack propagation law for this example was assumed to be the same as the first example. It can be observed as the SIF solutions presented in this paper are able to adequately reproduce the quick tendency

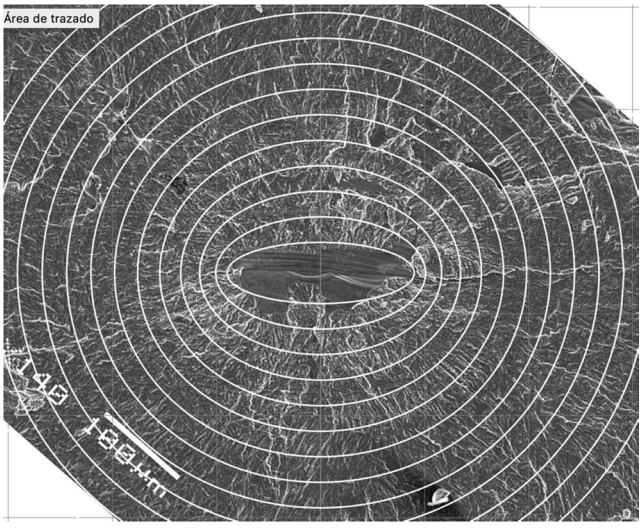

Fig. 8. First crack paths calculated from an initial defect with a large crack aspect ratio.

of the crack to growth from an initial defect with a high aspect ratio to a near circular crack. This feature is typical for the growth of a crack in this geometry. The crack front during propagation can be estimated from beach marks or from radial striations emanating from the initiating defects, which, although not true crack front marks, can be considered indications of the direction of crack front propagation.

Finally, Figs. 9 and 10 reproduce the fatigue tests conducted by de Jesus *et at.* [20]. The circular specimens were fabricated by SLM of Ti-6Al-4V alloy, and a centered penny-shaped initial defect was generated during printing. The fatigue tests were carried out under two different propagation conditions, (1) with a small channel linking the inner penny-shaped defect with the outer surface, which the authors termed as *in-air* conditions, and (2) with the embedded penny-shaped defect, which they call *in-vacuum* conditions. Included in these Figs. 9 and 10 are the corresponding fractographies and the evolution of the number of cycles versus crack size. The radius of the specimen was $R = 5$ mm, the uniaxial applied stress was $\Delta\sigma = 382$ MPa with a stress ratio of $\sigma_{min}/\sigma_{max} = 0$. The initial crack size was $a_0 = c_0 = 0.25$ mm, and the Paris law coefficients assumed for both conditions, were $C = 8.2{\cdot}10^{-8}$ and $m = 2.0$ for in-air conditions, and $C = 3.5{\cdot}10^{-8}$ and $m = 2.1$ for in-vacuum conditions, being ΔK in $MPa{\cdot}m^{1/2}$ and da/dN in $mm/cycle$. The control parameter for crack advance calculations was $\Delta a_1 = 0.005$ mm.

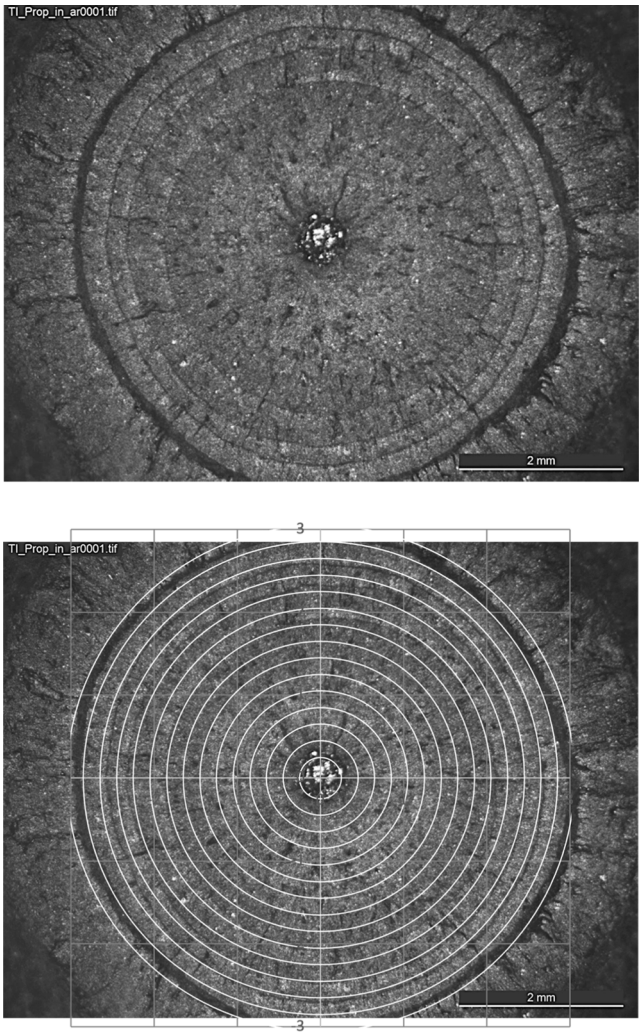

Fig. 9. Simulation using the present closed-form equations of the crack propagation path for a central crack specimens tested by Jesus et al. [20].

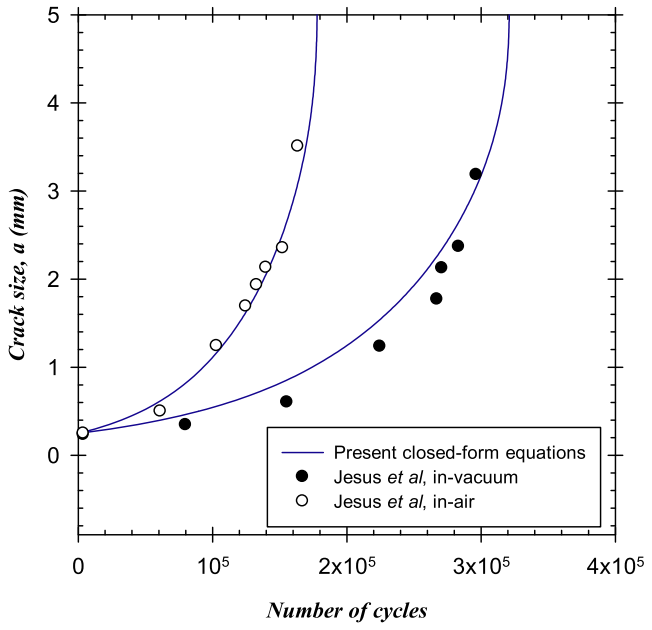

Fig. 10. Simulation using the present closed-form equations of the Crack size vs. number of cycles for two central crack specimens tested by Jesus et al. [20].

7. Conclusions

This paper presents a set of closed-form equations for the calculation of the SIF of elliptical embedded cracks in round bars subjected to tensile loads. Geometry correction factors are presented as a function of three dimensionless parameters, representative of the crack size, crack aspect ratio and crack position. A good fit is obtained when comparing the closed-form equations with the numerical tabulated values obtained from a 3D finite element calculation.

The simplified closed-form solution for an eccentric circular crack is also included, due to its practical application. Any irregular flaw in this geometry quickly develops a circular crack. This is a typical feature observed for the fatigue crack propagation emanating from internal defects in this geometry, and as a consequence, a simplified calculation of the crack propagation assuming a circular crack during propagation could be considered.

The present closed-form equations can be used for the simulation of the fatigue crack growth using a sequential methodology. This methodology allows the crack shape evolution to be updated during the fatigue process, assuming an elliptical crack shape evolution during propagation or a circular crack propagation for the simplified approach. A good estimation of fatigue crack growth can be carried out using the proposed SIF solutions, and the predictions are in good agreement with experiments conducted in fatigue specimens.

Declaration of Competing Interest

The authors declare that they have no known competing financial interests or personal relationships that could have appeared to influence the work reported in this paper.

Acknowledgements

The authors gratefully acknowledge financial support from the Junta de Castilla y Leon (Spain) through grant BU-002-P20, co-financed by FEDER funds.

References

[1] H.Q. Nguyen, L. Gallimard, C. Bathias, Numerical simulation of fish-eye fatigue crack growth in very high cycle fatigue, Eng. Fract. Mech. 135 (2015) 81–93, https://doi.org/10.1016/j.engfracmech.2015.01.010.
[2] Y. Hong, C. Sun, The nature and the mechanism of crack initiation and early growth for very-high-cycle fatigue of metallic materials – an overview, Theor. Appl. Fract. Mech. 92 (2017) 331–350, https://doi.org/10.1016/j.tafmec.2017.05.002.
[3] C. Stäcker, M. Sander, Experimental, analytical and numerical analyses of constant and variable amplitude loadings in the very high cycle fatigue regime, Theor. Appl. Fract. Mech. 92 (2017) 394–409, https://doi.org/10.1016/j.tafmec.2017.07.021.
[4] A.E. Green, I.N. Sneddon, The distribution of stress in the neighbourhood of a flat elliptical crack in an elastic solid, Math. Proc. Cambridge Philos. Soc. (1950), https://doi.org/10.1017/S0305004100025585.
[5] G.R. Irwin, Crack-extension force for a part-through crack in a plate, J. Appl. Mech. Trans. ASME. (1960), https://doi.org/10.1115/1.3640649.
[6] I.G.R. Tada H., P.C. Paris, The Stress Analysis of Cracks Handbook, 3rd ed., Del Research Corporation, Hellertown, 1973.
[7] I.V. Varfolomeev, V.A. Vainshtok, Calculation of stress intensity factors of embedded cracks in structural elements, Strength Mater. 20 (1988) 575–582, https://doi.org/10.1007/BF01528542.
[8] J.C. Newman, I.S. Raju, Stress-intensity factor equations for cracks in three-dimensional finite bodies subjected to tension and bending loads, NASA Tech. Memo. 85793, Lengley Res. Center, Hamton, VA, 1984. <https://ntrs.nasa.gov/archive/nasa/casi.ntrs.nasa.gov/19840015857.pdf>.
[9] M. Isida, H. Noguchi, Tension of a plate containing an embedded elliptical crack, Eng. Fract. Mech. 20 (1984) 387–408, https://doi.org/10.1016/0013-7944(84)90046-8.
[10] I.N. Sneddon, R.J. Tait, The effect of a penny-shaped crack on the distribution of stress in a long circular cylinder, Int. J. Eng. Sci. (1963), https://doi.org/10.1016/0020-7225(63)90016-8.
[11] M. Shariati, M.M. Rokhi, H. Rayegan, Investigation of stress intensity factor for internal cracks in FG cylinders under static and dynamic loading, Frat. Ed Integrita Strutt. 11 (2017) 166–180, https://doi.org/10.3221/IGF-ESIS.39.17.
[12] ASME-API, Fitness-for-Service API 579-1/ASME FFS-1, 2016.
[13] T. Nishioka, S.N. Atluri, Analytical solution for embedded elliptical cracks, and finite element alternating method for elliptical surface cracks, subjected to arbitrary loadings, Eng. Fract. Mech. 17 (1983) 247–268, https://doi.org/10.1016/0013-7944(83)90032-2.
[14] J.P. Benthem, W.T. Koiter, Asymptotic approximations to crack problems, Methods Anal. Solut. Crack Probl. (1973), https://doi.org/10.1007/978-94-017-2260-5_3.
[15] M. Kocak, S. Webster, J.J. Janosch, R.A. Ainsworth, R. Koers, FITNET Fitness-for-Service (FFS) Procedure, 2008.
[16] B. Pyttel, I. Varfolomeyev, C. Berger, FKM-guideline "fracture mechanics proof of strength for engineering components", Materwiss. Werksttech. (2007) https://doi.org/10.1002/mawe.200700134.
[17] J.M. Alegre, I.I. Cuesta, A. Díaz, Stress-intensity factor solutions for embedded elliptical cracks in round bars subjected to tensile load, Theor. Appl. Fract. Mech. 117 (2022) 103189, https://doi.org/10.1016/j.tafmec.2021.103189.
[18] Y. Murakami, S. Beretta, Small defects and inhomogeneities in fatigue strength: experiments, models and statistical implications, Extremes 2 (1999) 123–147.
[19] J.M. Alegre, I.I. Cuesta, A. Díaz, Stress-intensity factor solutions for the simulation of fish-eye fatigue crack growth in round bars subjected to tensile load, Proc. Struct. Integr. 39 (2022) 148–156.
[20] J. de Jesus, M. Borges, F. Antunes, J. Ferreira, L. Reis, C. Capela, A novel specimen produced by additive manufacturing for pure plane strain fatigue crack growth studies, Metals (Basel). 11 (2021), https://doi.org/10.3390/met11030433.